

# Experimental demonstration of a high-fidelity virtual two-qubit gate

Akhil Pratap Singh,<sup>1</sup> Kosuke Mitarai,<sup>2</sup> Yasunari Suzuki,<sup>3</sup> Kentaro Heya,<sup>4</sup> Yutaka Tabuchi,<sup>4</sup> Keisuke Fujii,<sup>2,4</sup> and Yasunobu Nakamura<sup>1,4</sup>

<sup>1</sup>*Department of Applied Physics, Graduate School of Engineering,  
The University of Tokyo, Bunkyo-ku, Tokyo, 113-8656, Japan*

<sup>2</sup>*Graduate School of Engineering Science, Osaka University 1-3 Machikaneyama, Toyonaka, Osaka 560-8531, Japan*

<sup>3</sup>*NTT Computer and Data Science Laboratories, NTT Corporation, Musashino 180-8585, Japan*

<sup>4</sup>*RIKEN Center for Quantum Computing (RQC), Wako, Saitama 351-0198, Japan*

We experimentally demonstrate a virtual two-qubit gate and characterize it using quantum process tomography (QPT). The virtual two-qubit gate decomposes an actual two-qubit gate into single-qubit operations and projective measurements in quantum circuits for expectation-value estimation. We implement projective measurements via mid-circuit dispersive readout. The deterministic sampling scheme reduces the number of experimental circuit evaluations required for decomposing a virtual two-qubit gate. We also apply measurement error mitigation to suppress the effect of readout errors and improve the average gate fidelity of a virtual controlled- $Z$  (CZ) gate to  $f_{av} = 0.9975 \pm 0.0028$ . Our results highlight a practical approach to implement virtual two-qubit gates with high fidelities, which are useful for simulating quantum circuits using fewer qubits and implementing two-qubit gates on a distant pair of qubits.

## I. INTRODUCTION

Quantum computing research is progressing on a promising yet challenging path to realize a scalable fault-tolerant quantum computer, which is expected to have the capabilities to solve many problems intractable for their classical counterparts. However, current quantum devices with limited coherence times, low scalability, and non-negligible noises, termed as noisy intermediate scale quantum, or NISQ devices [1], are still far from being a full-fledged quantum computer. Nevertheless, they are still proving to be the testbeds for many promising quantum algorithms and quantum applications [2–8]. The recent experimental demonstrations of quantum computation with over 50 qubits [9–12] have motivated the practical interest in solving large problems using smaller quantum devices, despite the trade-off of utilizing more classical resources.

To maximize the capabilities of a limited-sized NISQ quantum processor, various techniques for simulating large quantum circuits with smaller quantum devices have been proposed and demonstrated [13–19]. These techniques are useful for the expectation value estimation of a large quantum circuit, as they can reduce the hardware requirement by “cutting” the circuit, albeit with some overhead cost. Mitarai and Fujii [20] proposed the “virtual two-qubit gate” technique, a general decomposition scheme for a two-qubit gate. The virtual two-qubit gate allows us to simulate a two-qubit gate from a quasi-probability decomposition of local single-qubit operations in the quantum circuits used for the expectation value estimation for observables. The virtual two-qubit gate scheme has been experimentally utilized on a distant pair of superconducting qubits to reduce the number of SWAP operations required and thus reducing the two-qubit errors [21]. However, the characterization of the virtual two-qubit gate was not performed, thereby limiting the ability to evaluate its quality.

In this work, we experimentally demonstrate a virtual two-qubit gate taking the example of a controlled- $Z$  (CZ) gate and characterize it through the quantum process tomography (QPT) [22]. The virtual two-qubit gate requires the implementation of projection gates, which are non-unitary. We implement the projection gates through mid-circuit measurements. However, this limits the fidelity of the virtual two-qubit gate since measurement errors are typically higher than single-qubit gate errors. We thus formulate the measurement error mitigation for mid-circuit measurements and apply it to improve the average gate fidelity of the virtual two-qubit gate.

The rest of the paper is organized as follows: In Sec. II, we review the virtual two-qubit gate decomposition technique, and present our approach for its experimental implementation. We then discuss combining the measurement error mitigation with the virtual two-qubit gate. Section III provides details on the experimental device, gate implementation, and the characterization of the virtual CZ gate. We also demonstrate the improved average gate fidelity of the virtual CZ gate after incorporating the measurement error mitigation. Lastly, in Sec. IV we summarize our work and discuss potential directions for future work.

## II. METHODS

### A. Gate Decomposition

We can break down any two-qubit gate expressed in the form  $e^{i\theta A \otimes B}$  into six local single-qubit operations, where  $A^2 = B^2 = I$ , and  $I$  is an identity matrix. We use the tilde ( $\sim$ ) symbol to represent a superoperator  $\tilde{U}$  corresponding to an operator  $U$  whose action on a density matrix  $\rho$  is defined as  $\tilde{U}\rho = U\rho U^\dagger$ .

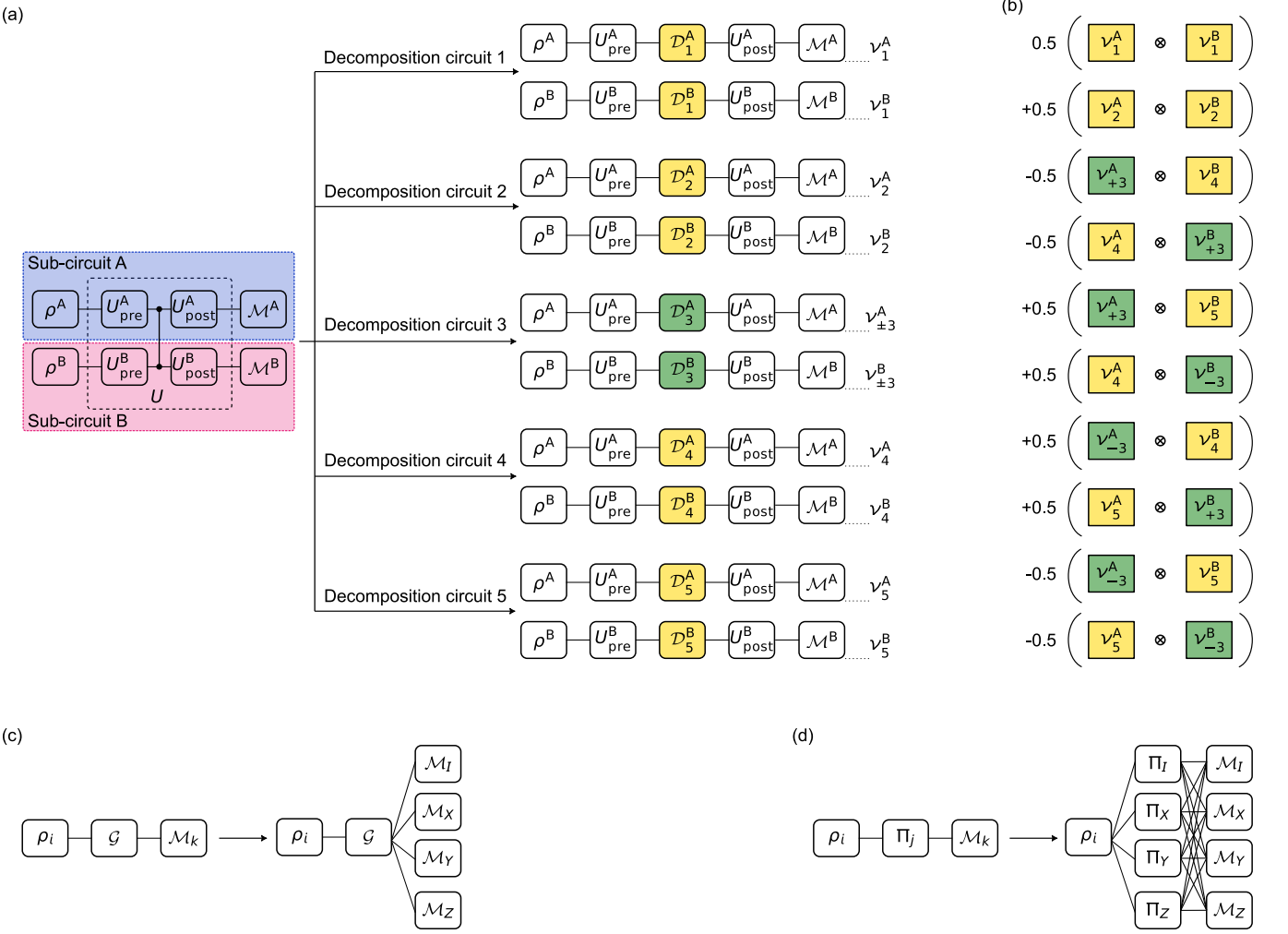


**FIG. 1: Decomposition of a CZ gate and measurement error mitigation.** (a) Decomposition of a simple two-qubit quantum circuit with a single CZ gate and other one-qubit gates. See text for the explanation. (b) Calculation of the final expectation value using the expectation values  $\nu_j^i$  obtained in the respective decomposition circuits in (a). (c) Measurement error mitigation for a single-qubit unitary operation. (d) Measurement error mitigation for a projection gate.

The decomposition of a CZ gate is written as

$$\begin{aligned} \widetilde{\text{CZ}} = & \frac{1}{2} \left( \tilde{\mathcal{R}}_Z \left( \frac{\pi}{2} \right) \otimes \tilde{\mathcal{R}}_Z \left( \frac{\pi}{2} \right) \right) \\ & + \frac{1}{2} \left( \tilde{\mathcal{R}}_Z \left( -\frac{\pi}{2} \right) \otimes \tilde{\mathcal{R}}_Z \left( -\frac{\pi}{2} \right) \right) \\ & - \frac{1}{2} \sum_{\alpha_1, \alpha_2} \alpha_1 \alpha_2 \left[ \tilde{\Pi}_{\alpha_1 Z} \otimes \tilde{\mathcal{R}}_Z \left( (\alpha_2 + 1) \frac{\pi}{2} \right) \right. \\ & \quad \left. + \tilde{\mathcal{R}}_Z \left( (\alpha_1 + 1) \frac{\pi}{2} \right) \otimes \tilde{\Pi}_{\alpha_2 Z} \right], \quad (1) \end{aligned}$$

where  $\alpha_1, \alpha_2 \in \{-1, +1\}$ .  $\tilde{\mathcal{R}}_Z(\pm\theta)$  and  $\tilde{\Pi}_{\pm Z}$  are superoperators corresponding to the operators  $\mathcal{R}_Z(\pm\theta) = e^{\pm i Z \theta / 2}$  and  $\Pi_{\pm Z} = (I \pm Z) / 2$ , respectively.  $\Pi_{\pm Z}$  are the (non-destructive) projection gates, which project the quantum state onto the respective eigenbasis and are

non-unitary [20].

Reference [20] has quantified the decomposition cost in terms of quasi-probability simulation where the decomposition operators in Eq. (1) are sampled with probabilities proportional to their coefficients [23]. The set of these decomposition operators can also be written as

$$\begin{aligned} \mathcal{D}_{\text{CZ}} = & \left\{ \mathcal{R}_Z \left( \frac{\pi}{2} \right) \otimes \mathcal{R}_Z \left( \frac{\pi}{2} \right), \mathcal{R}_Z \left( -\frac{\pi}{2} \right) \otimes \mathcal{R}_Z \left( -\frac{\pi}{2} \right), \right. \\ & \mathcal{R}_Z(\pi) \otimes \Pi_{\pm Z}, I \otimes \Pi_{\pm Z}, \Pi_{\pm Z} \otimes \mathcal{R}_Z(\pi), \\ & \left. \Pi_{\pm Z} \otimes I \right\}. \quad (2) \end{aligned}$$

In this work, we employ deterministic sampling for the decomposition operators, which means that we perform uniform experiments with each operator from Eq. (2) in a deterministic manner. Unlike the quasi-probability ap-

proach, we uniformly sample the decomposition operators with a probability of unity, regardless of their coefficients. We do that because of following two reasons. First, by implementing deterministic sampling, we can reduce the total number of circuit evaluations for each sub-circuit from six to five. It is explained in detail later in this section. Second, apart from the virtual two-qubit gate implementation, we also perform its characterization. To obtain the process matrix for the virtual CZ gate, we need process matrices of all the decomposition operators  $\mathcal{D}_j^i$  (see Sec. III B). Thus, we implement each decomposition operation deterministically.

Figure 1(a) illustrates the circuit decomposition for a virtual CZ gate in terms of experimental implementation. We consider a simple two-qubit quantum circuit consisting of single-qubit gates and a CZ gate. The aim here is to do the expectation value estimation for this two-qubit circuit using only one qubit by replacing an actual CZ gate with a virtual CZ gate. For the virtual two-qubit gate decomposition, we cut the CZ gate and consider the remaining circuit consisting of two one-qubit sub-circuits A and B. Each sub-circuit consists of the initial state  $\rho^i$ , set of single-qubit gates implemented before and after the CZ gates denoted by  $U_{\text{pre}}^i$  and  $U_{\text{post}}^i$ , respectively, and the measurement of observable  $k$ ,  $\mathcal{M}_k^i$ , where the superscript  $i \in \{\text{A}, \text{B}\}$  refers to the sub-circuit they belong to. In order to do the expectation value estimation using a virtual two-qubit gate, we do five different circuit evaluations, labelled as ‘‘Decomposition circuits’’ in Fig. 1(a), where we replace the actual CZ gate with local decomposition operators  $\mathcal{D}_j^i$  on both control and target qubits shown on the right hand side of Fig. 1(a). In  $\mathcal{D}_j^i$ ,  $i \in \{\text{A}, \text{B}\}$  and  $j \in \{1, 2, 3, 4, 5\}$  refer to the indices of the sub-circuits and the decomposition circuits, respectively. Single-qubit unitary operations  $\mathcal{D}_{j=1,2,4,5}^i \in \{\mathcal{R}_Z(\pi/2), \mathcal{R}_Z(-\pi/2), I, Z\}$  are shown in the yellow boxes, while projection gates  $\mathcal{D}_{j=3}^i = \{\Pi_{\pm Z}\}$  are shown in the green boxes. For the expectation value estimation using the virtual two-qubit gate, we substitute the expectation values  $\nu_j^i$  obtained from decomposition circuits 1–5 in Eq. (1) and get the final value as illustrated in Fig. 1(b).

Note that the utilization of the virtual two-qubit gate can allow us to decompose a quantum circuit  $U$  into two completely separate quantum circuits each acting only on qubits in sub-circuits A and B, as considered in Fig. 1(a). We take input to the circuit as a separable state  $\rho = \rho_A \otimes \rho_B$ . As an output, we wish to obtain expectation value  $P = P_A \otimes P_B$ , where  $P_A$  and  $P_B$  are Pauli operators acting on groups A and B, respectively. For example, if we define two superoperators  $\tilde{U}_1$  and  $\tilde{U}_2$  then their tensor product is expressed as

$$(\tilde{U}_1 \otimes \tilde{U}_2)\rho = (U_1 \otimes U_2)\rho(U_1^\dagger \otimes U_2^\dagger). \quad (3)$$

Using Eq. (3),  $U$ , as shown in Fig. 1(a), can be decomposed as

$$\tilde{U} = \sum_j c_j \left( \tilde{U}_{\text{post}}^{\text{A}} \otimes \tilde{U}_{\text{post}}^{\text{B}} \right) \left( \tilde{\mathcal{D}}_j^{\text{A}} \otimes \tilde{\mathcal{D}}_j^{\text{B}} \right) \left( \tilde{U}_{\text{pre}}^{\text{A}} \otimes \tilde{U}_{\text{pre}}^{\text{B}} \right), \quad (4)$$

where  $\{c_j\}$  are the coefficients of the corresponding decomposition operators  $\mathcal{D}_j^i$  [20]. The desired expectation value can be written as

$$\text{Tr} \left( P \tilde{U} \rho \right) = \sum_j c_j \left[ \text{Tr} \left( P_A \tilde{U}_{\text{post}}^{\text{A}} \tilde{\mathcal{D}}_j^{\text{A}} \tilde{U}_{\text{pre}}^{\text{A}} \rho_A \right) \right. \\ \left. \text{Tr} \left( P_B \tilde{U}_{\text{post}}^{\text{B}} \tilde{\mathcal{D}}_j^{\text{B}} \tilde{U}_{\text{pre}}^{\text{B}} \rho_B \right) \right]. \quad (5)$$

Therefore, in this case, we can estimate all of the values of  $\text{Tr} \left( P_A \tilde{U}_{\text{post}}^{\text{A}} \tilde{\mathcal{D}}_j^{\text{A}} \tilde{U}_{\text{pre}}^{\text{A}} \rho_A \right)$  and  $\text{Tr} \left( P_B \tilde{U}_{\text{post}}^{\text{B}} \tilde{\mathcal{D}}_j^{\text{B}} \tilde{U}_{\text{pre}}^{\text{B}} \rho_B \right)$  separately for  $j = 1, \dots, 5$  and then combine them according to Eq. (5) to obtain the result for  $U$ . We note that for quasi-probability sampling of the decomposition operations, Eq. (1) needs six different circuit evaluations because there are six distinct operations (see Eq. (2)) involved in Eq. (1). However, by comparing Eq. (1), Eq. (2), and Eq. (5), we see that if we sample the decomposition operators  $\mathcal{D}_j^i$  deterministically then we can reduce the total number of circuit evaluations for each sub-circuit from six to five. This can be done since, by implementing the projection gates through mid-circuit measurements, we obtain both expectation values of the projection operators ( $\Pi_{\pm Z}$  in case of a CZ gate) in a single experiment ( $\nu_{\pm 3}^{\text{A,B}}$  in Fig. 1(a)).

## B. Combining measurement error mitigation with the virtual two-qubit gate

We use mid-circuit measurements to implement the projection gates. The measurement errors become the dominant contributor to the average gate infidelity of the virtual two-qubit gate since the measurement errors (3.9%) are much larger than the initialization errors ( $\sim 1\%$ ) and single-qubit errors ( $< 0.05\%$ ) in our device. The details of the device are presented in Sec. III A. In order to mitigate the measurement errors, we perform quantum error mitigation (QEM) with the probabilistic error cancellation (PEC) method [24, 25]. In this method, we define a set of modified circuits for the original circuit in which we wish to mitigate the errors. Then, the original circuit is replaced randomly by a selected set of modified circuits, where the probabilities to select the random circuits are calculated before running the quantum circuits. The mitigated result is obtained by taking the average of the modified circuits. Here, we apply this error mitigation technique both to the mid-circuit measurements for the projection gates and to the final measurements. Figure 1(c) illustrates the measurement error mitigation circuit for single-qubit unitary operations

**TABLE I:** Parameters of the superconducting transmon qubit used in the experiments: the qubit frequency  $\omega_q$ , anharmonicity  $\alpha$ , energy relaxation time  $T_1$ , and Ramsey dephasing time  $T_2^*$ .

	$\omega_q/2\pi$	$\alpha/2\pi$	$T_1$	$T_2^*$
Qubit	8.403 GHz	-416 MHz	20.2 $\mu$ s	3.1 $\mu$ s

where  $\mathcal{G} = \mathcal{D}_{j=\{1,2,4,5\}}$ , and instead of the measurement of the desired observable  $k$ ,  $\mathcal{M}_k$ , we measure the set of Pauli operators denoted as  $\mathcal{M}_P = \mathcal{M}_{\{I,X,Y,Z\}}$ . In the experiments, measurements on the  $X$  and  $Y$  basis are implemented by applying  $\mathcal{R}_Y(\pi/2)$  and  $\mathcal{R}_X(\pi/2)$  gates, respectively, just before the usual  $Z$  basis measurement. For measurement in the  $I$  basis, we always consider the expectation value of operator  $I$  to be unity. In case of the projection gates  $\mathcal{D}_{j=3}$ , we apply the probabilistic measurement error mitigation sequentially [25], first on the mid-circuit measurement  $\Pi_j$  and then on the final measurement  $\mathcal{M}_k$  as shown in Fig. 1(d). See Appendix A for the details.

### III. EXPERIMENT

#### A. System details

Local single-qubit operations can be classified into two categories: unitary and non-unitary/projection gates. To implement a virtual CZ gate experimentally, we use a fixed-frequency superconducting transmon qubit [26]. The qubit is a part of a 16-qubit device [27]. The parameters of the qubit are summarized in Table I.

In experiments, the quantum gates and measurements are noisy, and thus we do not have perfect implementations of the above gates as mentioned in Eq. (1). Thus, hereafter we use the superscript “exp” to denote a quantum operation realized in the experiments and hence containing the errors. Let noisy quantum channels that correspond to  $Z$ ,  $\mathcal{R}_Z(\pm\theta)$  and  $\Pi_{\pm Z}$  be  $Z^{\text{exp}}$ ,  $\mathcal{R}_Z^{\text{exp}}(\pm\theta)$  and  $\Pi_{\pm Z}^{\text{exp}}$ , respectively. To implement  $\mathcal{R}_Z^{\text{exp}}(\pm\theta)$  and  $Z^{\text{exp}}$ , we use the efficient  $Z$ -gate technique [28], in which the rotation around the  $Z$ -axis can be executed by adjusting the relative phase of the subsequent  $X$  and  $Y$  qubit drive pulses, which is controlled through the classical hardware and software and can be implemented almost perfectly. The  $\mathcal{R}_X^{\text{exp}}(\pi/2)$ ,  $\mathcal{R}_Y^{\text{exp}}(\pi/2)$  gates are implemented with the shaped microwave pulses [29]. For suppressing leakage, we use the DRAG pulsing technique [30, 31]. To reduce the unitary control errors, we use the ORBIT technique [32]. The average gate fidelity of the single-qubit Clifford gates is  $0.9992 \pm 0.0004$  via randomized benchmarking [33–35].

To implement  $\Pi_{\pm Z}^{\text{exp}}$ , we perform dispersive readout [36] followed by classical post-processing. The qubit state is measured through an off-resonantly coupled resonator

with the dispersive readout performed via the readout resonator at 10.310 GHz. The readout signal is amplified with an impedance-matched Josephson parametric amplifier [37, 38]. The averaged assignment fidelity for the qubit readout is  $0.9609 \pm 0.0037$  (see more details in Appendix B).

#### B. Characterization and results

To represent quantum states, quantum channels, and measurements, we use the Pauli transfer matrix (PTM) representation. We define  $\sigma_k$  ( $k = 0, \dots, 3$ ) as the  $k$ th operator in the Pauli basis,  $\mathcal{P} = \{I, X, Y, Z\}$ . We define a quantum channel corresponding to a decomposition operation  $\mathcal{D} \in \mathcal{D}_j^i$  as  $\tilde{\mathcal{D}}$ . The PTM representation of a quantum channel  $\tilde{\mathcal{D}}$  can be written as  $T$ , whose elements are given by

$$T(\tilde{\mathcal{D}})_{k,l} = \frac{1}{d} \text{Tr} [\sigma_k \tilde{\mathcal{D}}(\sigma_l)], \quad (6)$$

where  $d = 2^n$  is the dimension of the  $n$ -qubit system. For the virtual CZ gate characterization, we perform QPT. Figure 1(a) also represents the circuit for virtual two-qubit gate QPT, where we perform QPT in each sub-circuit for the corresponding decomposition channel  $\tilde{\mathcal{D}}_{j=1,\dots,5}^{i=A,B}$ . As per the QPT procedure, we prepare  $d^2 = 4$  linearly independent states from the basis  $\rho_{\text{in}}^{i=A,B} = \{|0\rangle, |1\rangle, |+\rangle, |i+\rangle\}$ , each of which is subjected to the quantum channel  $\tilde{\mathcal{D}}_j^i$ , followed by the quantum state tomography (QST) [2], which includes measurements of the  $\{X, Y, Z\}$  observables. Here, we have denoted  $|\pm\rangle$ ,  $|i\pm\rangle$ , and  $|0\rangle$  and  $|1\rangle$  as the eigenvectors of  $X$ ,  $Y$ , and  $Z$  with eigenvalues  $\pm 1$ , respectively. Since we are interested in the QPT of  $\tilde{\mathcal{D}}_j^i$ , we take corresponding  $U_{\text{pre,post}}^{i=A,B}$  to be the identity gates  $I^A$  and  $I^B$ . These set of experiments constitute a QPT circuit evaluation for the channel  $\tilde{\mathcal{D}}_j^i$ . After obtaining  $T(\tilde{\mathcal{D}}_j^i)$  for both sub-circuits A and B, we use Eq. (1) to calculate the PTM for the virtual CZ gate  $T_{V-CZ}$ . See Appendix C.

We present the characterization results for the virtual CZ gate and compare the cases with (PEC) and without (non-PEC) measurement error mitigation in Fig. 2. For each QPT circuit evaluation of  $\tilde{\mathcal{D}}_j^i$  in PEC experiments, we take  $N_s = 10,000$  shots to calculate the average expectation value for the corresponding observables  $\mathcal{M}_{k=\{X,Y,Z\}}$ . In PEC experiments, we replace each  $\mathcal{M}_k$  with the measurement set of Pauli observables  $\mathcal{M}_p \in \{\mathcal{M}_I, \mathcal{M}_X, \mathcal{M}_Y, \mathcal{M}_Z\}$  as shown in Fig. 1(c)–(d). See Appendix A for the details. To get the final mitigated expectation value with its uncertainty, we repeat each QPT circuit 100 times and take its average. To obtain the non-PEC QPT data, we use the data samples obtained in the PEC QPT experiments but only selecting the data samples where,  $\mathcal{M}_p = \mathcal{M}_k$ . We use the same data samples to avoid any possibility of time-dependent errors between different circuit operations. Because of

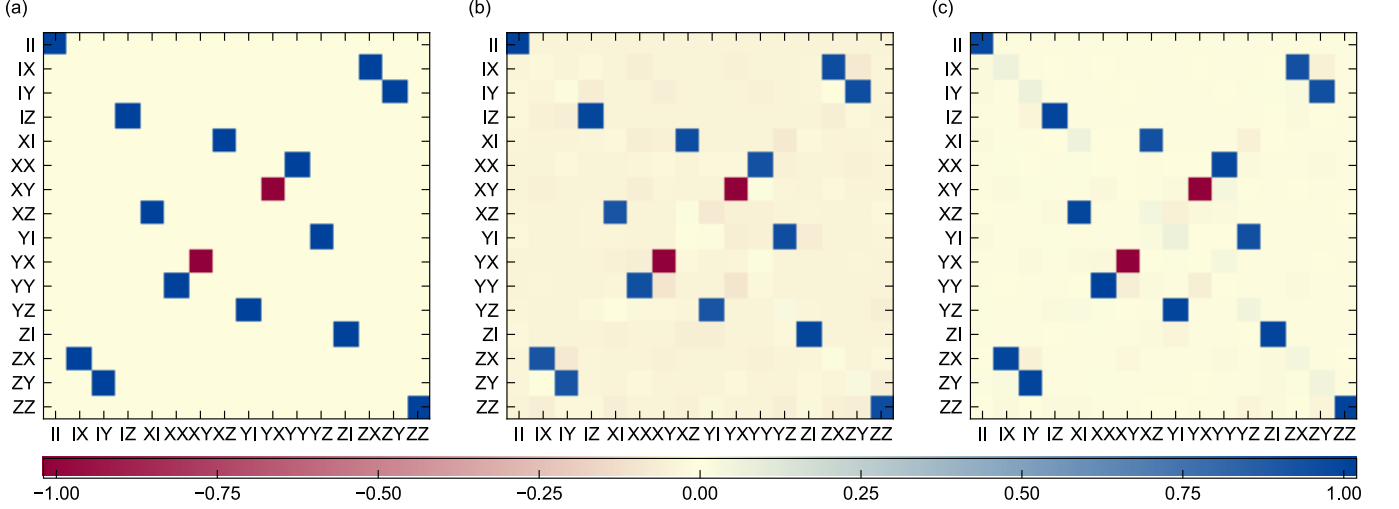


**FIG. 2: Quantum process tomography results for a CZ gate.** (a) Ideal CZ gate in the Pauli transfer matrix representation. (b) Experimentally-implemented virtual CZ gate without measurement error mitigation. (c) Experimentally-implemented virtual CZ gate with measurement error mitigation.

that, the total number of shots for the non-PEC QPT experiments  $N_r$  vary slightly since they are obtained probabilistically. For all the 100 repetitions the range of the  $N_r$  is  $8709 \leq N_r \leq 9869$ . The average gate fidelity for the virtual CZ gate without doing the measurement error mitigation is  $f_{av} = 0.9329 \pm 0.0021$ , and after applying the measurement error mitigation it is improved to  $f_{av}^{mit} = 0.9975 \pm 0.0028$ , where “mit” denotes the fidelity after applying the PEC mitigation. The results indicate a feasible and practical approach to experimentally implement virtual two-qubit gates with enhanced fidelity by employing measurement error techniques for the projection gates performed through mid-circuit measurements and implementing high-fidelity local single-qubit gates. The high-fidelity virtual two-qubit gates are crucial for simulating quantum circuits using fewer qubits and also to simulate two-qubit gates on a distant pair of qubits which otherwise would take several number of SWAP operations between them.

#### IV. CONCLUSION AND DISCUSSION

In this work, we have experimentally demonstrated a virtual CZ gate and characterized it through QPT. By implementing probabilistic error cancellation, we mitigated the measurement errors and showed considerable improvement in the average gate fidelity of the virtual CZ gate despite that the measurement errors were much higher than the single-qubit gate errors. In one of the applications of the virtual two-qubit gates, where we broke a  $2N$ -qubit circuit into two disconnected  $N$ -qubit circuits, we reduced the number of circuit evaluations for each  $N$ -qubit circuit from six to five.

Decomposing a larger quantum circuit into smaller circuits can boost the capabilities of the limited-sized

NISQ devices which can pave the way towards the goal of demonstrating the quantum advantage. However, decomposing a quantum circuit requires large overhead in terms of additional number of circuit evaluations and classical post-processing. These costs vary depending on the decomposition techniques and the requirement of added classical resources. It would be interesting to explore a general approach to decompose a quantum circuit optimally which can also be implemented efficiently in the experiments.

#### ACKNOWLEDGEMENTS

We acknowledge Jesper Ilves, Takanori Sugiyama, and Shuhei Tamate for fruitful discussions. This work was partly supported by MEXT Q-LEAP (No. JPMXS0118068682), JST PRESTO (No. JPMJPR1916 and No. JPMJPR2015), JST Moonshot R&D (No. JPMJMS2061 and No. JPMJMS2067), JST ERATO (No. JPMJER1601), JSPS KAKENHI (No. JP22H05000 and No. JP22K17868), MEXT Q-LEAP (No. JPMXS0118067394), and JST COI- NEXT (No. JPMJPF2014).

#### Appendix A: Measurement error mitigation

We use the same approach for measurement QEM, first by obtaining the Gram matrix  $\mathbb{G}$  and then calculating the quasi-probabilities, as demonstrated in Ref. [25]. The Gram matrix  $\mathbb{G}^{\text{exp}}$ , as shown in Fig. A1(a), can be obtained experimentally by running the QPT circuits for an identity gate  $I$  and vectorizing the output states in the Pauli basis. We take the initial states as  $\rho_i = \{|0\rangle, |1\rangle, |+\rangle, |i+\rangle\}$  and the observables as  $\sigma_k$ ,

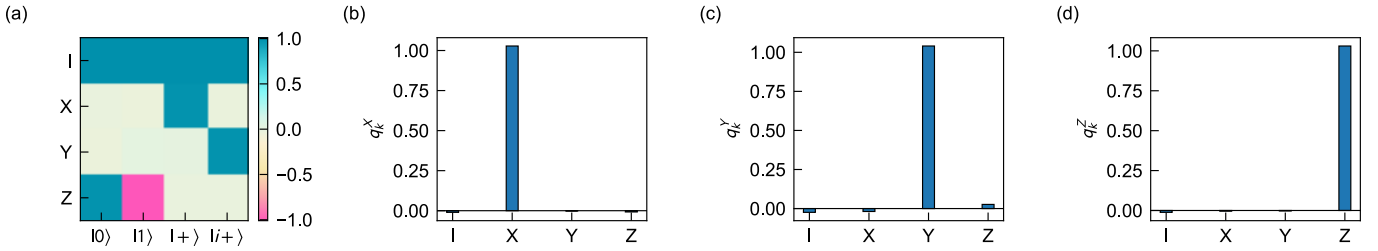


**FIG. A1: Gram matrix and quasi-probability vectors.** (a) Gram matrix for a single-qubit measurement. (b)–(d) Quasi-probability vectors for measurement basis  $X$ ,  $Y$ , and  $Z$ , respectively.

which are the  $k$ th elements of the Pauli basis  $\mathcal{P}$ . The set of initial states can be expressed as the state preparation matrix  $A^{\text{exp}}$  with its elements  $A_{k,i}^{\text{exp}} = \langle \langle \sigma_k | \rho_i^{\text{exp}} \rangle \rangle$  and the set of observables as the readout matrix  $B^{\text{exp}}$  with its elements  $B_{k,i}^{\text{exp}} = \langle \langle \sigma_k^{\text{exp}} | \sigma_i \rangle \rangle$ . To obtain  $B^{\text{exp}}$ , we use the relation,  $\mathbb{G}^{\text{exp}} = B^{\text{exp}} A^{\text{exp}}$ . Since, the state preparation errors are much lower in our device, we assume the state preparation to be almost perfect and take its estimate as error-free  $A^{\text{est}} = \langle \langle \sigma_k | \rho_i \rangle \rangle$  where “est” superscript denotes the estimate. With this, we can get the estimated readout matrix  $B^{\text{est}} = \mathbb{G}^{\text{exp}} (A^{\text{est}})^{-1}$ .

For the implementation of the PEC method, we need to find the quasi-probability vectors  $q_k$  corresponding to the measurement of the observable  $\mathcal{M}_k$ , which are expressed as

$$q_k = \langle \langle \mathcal{M}_k | (B^{\text{est}})^{-1} \rangle \rangle. \quad (\text{A1})$$

For example, in the QPT experiments, as also mentioned in Sec. III B, we need to do measurements of the observables  $\{X, Y, Z\}$  denoted as  $\mathcal{M}_{k=\{X,Y,Z\}}$ . Each observable  $\mathcal{M}_k$  can be expressed in terms of Pauli basis as

$$\mathcal{M}_k = \sum_l q_k^l \sigma_l, \quad (\text{A2})$$

where  $q_k^l$  are the elements of the quasi-probability vector  $q_k$ . Each observable  $\sigma_l$  is then measured with the probability  $p_k^l$  expressed as

$$p_k^l = \frac{|q_k^l|}{\sum_m |q_k^m|}. \quad (\text{A3})$$

The quasi-probability vectors  $q_{k=\{X,Y,Z\}}$  are shown in Figs. A1(b)–(d), respectively. In the case of  $\sigma_0 = I$ , we always consider the expectation value as +1. Each expectation value is multiplied by its weight,  $w_k^l = \text{sgn}(q_k^l) \sum_m |q_k^m|$ . This weighted average is the mitigated expectation value for the observable  $\mathcal{M}_k$ , which can be written as

$$\langle \mathcal{M}_k \rangle^{\text{mit}} = \sum_l w_k^l \langle \mathcal{M}_k \rangle^{\text{exp}}, \quad (\text{A4})$$

where “mit” superscript denotes the error-mitigated expectation value.

To obtain the mitigated expectation values for the circuits containing projection gates  $\Pi_j$ , we perform the PEC

method sequentially first for the mid-circuit measurement observable  $\mathcal{M}'_j$  and then for the final measurement of the observable  $\mathcal{M}_k$ . Using Eqs. (A1) to (A3), we can see that  $\mathcal{M}'_j$  can be replaced by the Pauli operators  $\sigma_r$  with the probability

$$p_j^{r'} = \frac{|q_j^{r'}|}{\sum_s |q_j^{s'}|}. \quad (\text{A5})$$

The weight factors in this case are

$$w_{j,k}^{r',l} = \text{sgn}(q_j^{r'} \cdot q_k^l) \sum_s |q_j^{s'}| \cdot \sum_m |q_k^m|, \quad (\text{A6})$$

and the final expectation value is

$$\langle \mathcal{M}_{j',k} \rangle^{\text{mit}} = \sum_{r,l} w_{j,k}^{r',l} \langle \mathcal{M}_{j',k} \rangle^{\text{exp}}. \quad (\text{A7})$$

## Appendix B: Qubit readout characterization

To obtain the average assignment fidelity of the single-shot readout, we apply a  $\mathcal{R}_X(\pi/2)$  gate on the initial ground state  $|0\rangle$  and then apply two sequential measurement pulses. The average assignment fidelity is defined as

$$\mathcal{F}_a = \frac{1}{2} (p(g|g) + p(e|e)), \quad (\text{B1})$$

where  $p(x|y)$  is the probability of assigning the measurement outcome  $x$  when the qubit is prepared in the state  $y$ . We obtain the assignment fidelity of  $0.9609 \pm 0.0037$  and the ground-state initialization fidelity  $\mathcal{F}_{\text{init}} = p(g|g)$  of  $0.9895 \pm 0.0028$ .

## Appendix C: Quantum process tomography

We use QPT to evaluate the performance of the virtual two-qubit gate. In general, for a  $n$ -qubit system with the dimension  $d = 2^n$ , we can express a quantum channel  $\tilde{\mathcal{E}}$  acting on an arbitrary quantum state  $\rho$  as

$$\tilde{\mathcal{E}}(\rho) = \sum_{i,j=0}^{d^2-1} \chi_{ij} B_i \rho B_j^\dagger, \quad (\text{C1})$$

where  $\{B_i\}$  are the elements of the  $d \times d$  matrix basis and  $\chi$  is the process matrix [2]. We define the PTM representation of a quantum channel  $\tilde{\mathcal{E}}$  as  $T$ , whose elements are expressed as

$$T(\tilde{\mathcal{E}})_{i,j} = \text{Tr} [\sigma_i \tilde{\mathcal{E}}(\sigma_j)]. \quad (\text{C2})$$

In the PTM representation, we can express a state  $\rho$  as a column vector  $|\rho\rangle\rangle$  with elements  $|\rho\rangle\rangle_k = \text{Tr} [\sigma_k \rho]$  and an operator  $\mathcal{O}$  as a row vector  $\langle\langle \mathcal{O}|$  with elements  $\langle\langle \mathcal{O}|_k = \text{Tr} [\sigma_k \mathcal{O}]$ . In the QPT, we prepare for each qubit an initial state from the set  $\{|0\rangle, |1\rangle, |+\rangle, |i+\rangle\}$ . For each initial state, we measure the qubit along the Pauli basis,  $X$ ,  $Y$ , and  $Z$ .

Using the PTM representation, we can define the quantum channel for the two-qubit system as the tensor product of individual PTMs. Using Eqs. (1) and (6), we can express the PTM for the virtual CZ gate  $T_{V-CZ}$  as

$$T_{V-CZ} = \frac{1}{2} \sum_{i=1,2} \left( T(\tilde{\mathcal{D}}_i^A) \otimes T(\tilde{\mathcal{D}}_i^B) \right) - \frac{1}{2} \sum_{\alpha_1, \alpha_2, \beta} \alpha_1, \alpha_2 \left[ \left( T(\tilde{\mathcal{D}}_{\alpha_1 3}^A) \otimes T(\tilde{\mathcal{D}}_{\beta}^B) \right) + \left( T(\tilde{\mathcal{D}}_{\beta}^A) \otimes T(\tilde{\mathcal{D}}_{\alpha_2 3}^B) \right) \right], \quad (\text{C3})$$

where  $\alpha_1, \alpha_2 \in \{\pm 1\}$  and  $\beta \in \{4, 5\}$ .

- [1] J. Preskill, Quantum Computing in the NISQ era and beyond, *Quantum* **2**, 79 (2018).
- [2] M. A. Nielsen and I. L. Chuang, *Quantum Computation and Quantum Information: 10th Anniversary Edition* (Cambridge University Press, 2010).
- [3] K. Bharti, A. Cervera-Lierta, T. H. Kyaw, T. Haug, S. Alperin-Lea, A. Anand, M. Degroote, H. Heimonen, J. S. Kottmann, T. Menke, W.-K. Mok, S. Sim, L.-C. Kwek, and A. Aspuru-Guzik, Noisy intermediate-scale quantum algorithms, *Rev. Mod. Phys.* **94**, 015004 (2022).
- [4] A. Peruzzo, J. McClean, P. Shadbolt, M.-H. Yung, X.-Q. Zhou, P. J. Love, A. Aspuru-Guzik, and J. L. O'Brien, A variational eigenvalue solver on a photonic quantum processor, *Nature Communications* **5**, 4213 (2014).
- [5] A. Montanaro, Quantum speedup of monte carlo methods, *Proc. R. Soc. A.* **471**, 20150301 (2015).
- [6] M. Cerezo, A. Arrasmith, R. Babbush, S. C. Benjamin, S. Endo, K. Fujii, J. R. McClean, K. Mitarai, X. Yuan, L. Cincio, and P. J. Coles, Variational quantum algorithms, *Nature Reviews Physics* **3**, 625 (2021).
- [7] Y. Cao, J. Romero, J. P. Olson, M. Degroote, P. D. Johnson, M. Kieferová, I. D. Kivlichan, T. Menke, B. Peropadre, N. P. D. Sawaya, S. Sim, L. Veis, and A. Aspuru-Guzik, Quantum chemistry in the age of quantum computing, *Chemical Reviews* **119**, 10856 (2019).
- [8] S. McArdle, S. Endo, A. Aspuru-Guzik, S. C. Benjamin, and X. Yuan, Quantum computational chemistry, *Rev. Mod. Phys.* **92**, 015003 (2020).
- [9] F. Arute, K. Arya, R. Babbush, D. Bacon, J. C. Bardin, R. Barends, R. Biswas, S. Boixo, F. G. S. L. Brandao, D. A. Buell, B. Burkett, Y. Chen, Z. Chen, B. Chiaro, R. Collins, W. Courtney, A. Dunsworth, E. Farhi, B. Foxen, A. Fowler, C. Gidney, M. Giustina, R. Graff, K. Guerin, S. Habegger, M. P. Harrigan, M. J. Hartmann, A. Ho, M. Hoffmann, T. Huang, T. S. Humble, S. V. Isakov, E. Jeffrey, Z. Jiang, D. Kafri, K. Kechedzhi, J. Kelly, P. V. Klimov, S. Knysh, A. Korotkov, F. Kostritsa, D. Landhuis, M. Lindmark, E. Lucero, D. Lyakh, S. Mandrà, J. R. McClean, M. McEwen, A. Megrant, X. Mi, K. Michelsen, M. Mohseni, J. Mutus, O. Naaman, M. Neeley, C. Neill, M. Y. Niu, E. Ostby, A. Petukhov, J. C. Platt, C. Quintana, E. G. Rieffel, P. Roushan, N. C. Rubin, D. Sank, K. J. Satzinger, V. Smelyanskiy, K. J. Sung, M. D. Trevithick, A. Vainsencher, B. Villalonga, T. White, Z. J. Yao, P. Yeh, A. Zalcman, H. Neven, and J. M. Martinis, Quantum supremacy using a programmable superconducting processor, *Nature* **574**, 505 (2019).
- [10] Y. Wu, W.-S. Bao, S. Cao, F. Chen, M.-C. Chen, X. Chen, T.-H. Chung, H. Deng, Y. Du, D. Fan, M. Gong, C. Guo, C. Guo, S. Guo, L. Han, L. Hong, H.-L. Huang, Y.-H. Huo, L. Li, N. Li, S. Li, Y. Li, F. Liang, C. Lin, J. Lin, H. Qian, D. Qiao, H. Rong, H. Su, L. Sun, L. Wang, S. Wang, D. Wu, Y. Xu, K. Yan, W. Yang, Y. Yang, Y. Ye, J. Yin, C. Ying, J. Yu, C. Zha, C. Zhang, H. Zhang, K. Zhang, Y. Zhang, H. Zhao, Y. Zhao, L. Zhou, Q. Zhu, C.-Y. Lu, C.-Z. Peng, X. Zhu, and J.-W. Pan, Strong quantum computational advantage using a superconducting quantum processor, *Phys. Rev. Lett.* **127**, 180501 (2021).
- [11] Q. Zhu, S. Cao, F. Chen, M.-C. Chen, X. Chen, T.-H. Chung, H. Deng, Y. Du, D. Fan, M. Gong, C. Guo, C. Guo, S. Guo, L. Han, L. Hong, H.-L. Huang, Y.-H. Huo, L. Li, N. Li, S. Li, Y. Li, F. Liang, C. Lin, J. Lin, H. Qian, D. Qiao, H. Rong, H. Su, L. Sun, L. Wang, S. Wang, D. Wu, Y. Wu, Y. Xu, K. Yan, W. Yang, Y. Yang, Y. Ye, J. Yin, C. Ying, J. Yu, C. Zha, C. Zhang, H. Zhang, K. Zhang, Y. Zhang, H. Zhao, Y. Zhao, L. Zhou, C.-Y. Lu, C.-Z. Peng, X. Zhu, and J.-W. Pan, Quantum computational advantage via 60-qubit 24-cycle random circuit sampling, *Science Bulletin* **67**, 240 (2022).

[12] Y. Kim, A. Eddins, S. Anand, K. X. Wei, E. van den Berg, S. Rosenblatt, H. Nayfeh, Y. Wu, M. Zaletel, K. Temme, and A. Kandala, Evidence for the utility of quantum computing before fault tolerance, *Nature* **618**, 500 (2023).

[13] S. Bravyi, G. Smith, and J. A. Smolin, Trading classical and quantum computational resources, *Phys. Rev. X* **6**, 021043 (2016).

[14] T. Peng, A. W. Harrow, M. Ozols, and X. Wu, Simulating large quantum circuits on a small quantum computer, *Phys. Rev. Lett.* **125**, 150504 (2020).

[15] C. Ying, B. Cheng, Y. Zhao, H.-L. Huang, Y.-N. Zhang, M. Gong, Y. Wu, S. Wang, F. Liang, J. Lin, Y. Xu, H. Deng, H. Rong, C.-Z. Peng, M.-H. Yung, X. Zhu, and J.-W. Pan, Experimental simulation of larger quantum circuits with fewer superconducting qubits, *Phys. Rev. Lett.* **130**, 110601 (2023).

[16] A. Eddins, M. Motta, T. P. Gujarati, S. Bravyi, A. Mezzacapo, C. Hadfield, and S. Sheldon, Doubling the size of quantum simulators by entanglement forging, *PRX Quantum* **3**, 010309 (2022).

[17] C. Piveteau and D. Sutter, Circuit knitting with classical communication (2022), [arXiv:2205.00016](https://arxiv.org/abs/2205.00016).

[18] L. Brenner, C. Piveteau, and D. Sutter, Optimal wire cutting with classical communication (2023), [arXiv:2302.03366](https://arxiv.org/abs/2302.03366).

[19] K. Fujii, K. Mizuta, H. Ueda, K. Mitarai, W. Mizukami, and Y. O. Nakagawa, Deep variational quantum eigensolver: A divide-and-conquer method for solving a larger problem with smaller size quantum computers, *PRX Quantum* **3**, 010346 (2022).

[20] K. Mitarai and K. Fujii, Constructing a virtual two-qubit gate by sampling single-qubit operations, *New Journal of Physics* **23**, 023021 (2021).

[21] T. Yamamoto and R. Ohira, Error suppression by a virtual two-qubit gate, *Journal of Applied Physics* **133**, 10.1063/5.0151037 (2023), 174401.

[22] J. M. Chow, J. M. Gambetta, L. Tornberg, J. Koch, L. S. Bishop, A. A. Houck, B. R. Johnson, L. Frunzio, S. M. Girvin, and R. J. Schoelkopf, Randomized benchmarking and process tomography for gate errors in a solid-state qubit, *Phys. Rev. Lett.* **102**, 090502 (2009).

[23] S. Hakkaku, Y. Tashima, K. Mitarai, W. Mizukami, and K. Fujii, Quantifying fermionic nonlinearity of quantum circuits, *Phys. Rev. Res.* **4**, 043100 (2022).

[24] S. Endo, S. C. Benjamin, and Y. Li, Practical quantum error mitigation for near-future applications, *Phys. Rev. X* **8**, 031027 (2018).

[25] C. Song, J. Cui, H. Wang, J. Hao, H. Feng, and Y. Li, Quantum computation with universal error mitigation on a superconducting quantum processor, *Science Advances* **5**, eaaw5686 (2019).

[26] J. Koch, T. M. Yu, J. Gambetta, A. A. Houck, D. I. Schuster, J. Majer, A. Blais, M. H. Devoret, S. M. Girvin, and R. J. Schoelkopf, Charge-insensitive qubit design derived from the cooper pair box, *Phys. Rev. A* **76**, 042319 (2007).

[27] S. Tamate, Y. Tabuchi, L. Szikszai, K. Kusuyama, K. Zuo, Z. Yan, A. Badruttinov, Y. Hishida, W. Qiu, H. Terai, G. Fujii, K. Makise, N. Watanabe, H. Nakagawa, M. Fujino, M. Ukibe, W. Mizubayashi, K. Kikuchi, and Y. Nakamura, Scalable packaging design for large-scale superconducting quantum circuit, *Bull. Am. Phys. Soc.* **66**, C30.9 (2021).

[28] D. C. McKay, C. J. Wood, S. Sheldon, J. M. Chow, and J. M. Gambetta, Efficient  $z$  gates for quantum computing, *Phys. Rev. A* **96**, 022330 (2017).

[29] E. Lucero, J. Kelly, R. C. Bialczak, M. Lenander, M. Mariantoni, M. Neeley, A. D. O'Connell, D. Sank, H. Wang, M. Weides, J. Wenner, T. Yamamoto, A. N. Cleland, and J. M. Martinis, Reduced phase error through optimized control of a superconducting qubit, *Phys. Rev. A* **82**, 042339 (2010).

[30] F. Motzoi, J. M. Gambetta, P. Rebentrost, and F. K. Wilhelm, Simple pulses for elimination of leakage in weakly nonlinear qubits, *Phys. Rev. Lett.* **103**, 110501 (2009).

[31] Z. Chen, J. Kelly, C. Quintana, R. Barends, B. Campbell, Y. Chen, B. Chiaro, A. Dunsworth, A. G. Fowler, E. Lucero, E. Jeffrey, A. Megrant, J. Mutus, M. Neeley, C. Neill, P. J. J. O'Malley, P. Roushan, D. Sank, A. Vainsencher, J. Wenner, T. C. White, A. N. Korotkov, and J. M. Martinis, Measuring and suppressing quantum state leakage in a superconducting qubit, *Phys. Rev. Lett.* **116**, 020501 (2016).

[32] J. Kelly, R. Barends, B. Campbell, Y. Chen, Z. Chen, B. Chiaro, A. Dunsworth, A. G. Fowler, I.-C. Hoi, E. Jeffrey, A. Megrant, J. Mutus, C. Neill, P. J. J. O'Malley, C. Quintana, P. Roushan, D. Sank, A. Vainsencher, J. Wenner, T. C. White, A. N. Cleland, and J. M. Martinis, Optimal quantum control using randomized benchmarking, *Phys. Rev. Lett.* **112**, 240504 (2014).

[33] E. Knill, D. Leibfried, R. Reichle, J. Britton, R. B. Blakestad, J. D. Jost, C. Langer, R. Ozeri, S. Seidelin, and D. J. Wineland, Randomized benchmarking of quantum gates, *Phys. Rev. A* **77**, 012307 (2008).

[34] J. Emerson, R. Alicki, and K. Życzkowski, Scalable noise estimation with random unitary operators, *Journal of Optics B: Quantum and Semiclassical Optics* **7**, S347 (2005).

[35] E. Magesan, J. M. Gambetta, and J. Emerson, Scalable and robust randomized benchmarking of quantum processes, *Phys. Rev. Lett.* **106**, 180504 (2011).

[36] A. Blais, R.-S. Huang, A. Wallraff, S. M. Girvin, and R. J. Schoelkopf, Cavity quantum electrodynamics for superconducting electrical circuits: An architecture for quantum computation, *Phys. Rev. A* **69**, 062320 (2004).

[37] J. Y. Mutus, T. C. White, R. Barends, Y. Chen, Z. Chen, B. Chiaro, A. Dunsworth, E. Jeffrey, J. Kelly, A. Megrant, C. Neill, P. J. J. O'Malley, P. Roushan, D. Sank, A. Vainsencher, J. Wenner, K. M. Sundqvist, A. N. Cleland, and J. M. Martinis, Strong environmental coupling in a Josephson parametric amplifier, *Appl. Phys. Lett.* **104**, 263513 (2014).

[38] Y. Urade, K. Zuo, S. Baba, C. Chang, K.-i. Nittoh, K. Inomata, Z. Lin, T. Yamamoto, and Y. Nakamura, Flux-driven impedance-matched Josephson parametric amplifier with improved pump efficiency, *Bull. Am. Phys. Soc.* **66**, A28.10 (2021).